OPEN ACCESS

REGULAR ARTICLE

Controlled Deposition of ZnO Thin Films by Spin Coating: Influence of Spin Speed on Film Microstructure and Transparency

M. Baneto^{1,2,* \infty}, D. Djagbai^{1,2}, E. Mouzou^{1,2,3}, A.D. Gboglo^{1,2}, O. Ako^{1,2}, M.F. Kouide^{1,2}, D. Kassegne^{1,2}

Centre d'Excellence Régional pour la Maîtrise de l'Electricité (CERME), University of Lomé, 01BP 1515 Lomé, Togo
 Laboratory on Solar Energy, Department of Physics, Faculty of Sciences, University of Lomé, 01BP 1515 Lomé, Togo
 Physics of Semiconductor Materials and Components Laboratory, Department of Physics, Faculty of Sciences,
 University of Lomé, 01BP 1515 Lomé, Togo

(Received 20 August 2025; revised manuscript received 18 October 2025; published online 30 October 2025)

Zinc oxide (ZnO) thin films were synthesized on glass substrates using the sol–gel spin coating method to investigate the effect of substrate rotation speed on their structural, morphological, and optical properties. Zinc acetate dihydrate, 2-methoxyethanol, and monoethanolamine were used as precursor, solvent, and stabilizer, respectively. The coating process was performed at spin speeds ranging from 1500 to 6500 rpm for 40 seconds. The films were subsequently preheated at 200 °C for 10 minutes and annealed at 400 °C for 3 hours. X-ray diffraction analysis confirmed that all films exhibited a polycrystalline hexagonal wurtzite structure. Scanning electron microscopy revealed that film morphology was significantly influenced by spin speed: low-speed coatings resulted in rough, heterogeneous surfaces, while higher speeds (\geq 4500 rpm) produced smooth, uniform films. UV–Vis spectroscopy showed that all samples maintained high transparency (above 70 %) in the visible region, with the highest transmittance (85 %) observed at 6500 rpm. The optical band gap varied between 3.28 and 3.32 eV depending on the spin speed. These results highlight the suitability of spin-coated ZnO thin films for transparent electrode applications in photovoltaic devices.

Keywords: Thin films, Zinc oxide, Microstructure, Spin coating, Spin speed, Photovoltaic applications.

DOI: 10.21272/jnep.17(5).05016 PACS numbers: 61.72. – y, 73.50.Pz

1. INTRODUCTION

Next-generation photovoltaic cells rely heavily on transparent semiconducting materials capable transmitting light and efficiently transporting charge carriers. Among these, Transparent Conductive Oxides (TCOs) serve a central function as electron transport layers in photovoltaic devices, especially in organic solar cells [1]. These materials are highly regarded for their excellent transparency in the visible spectrum, high electrical conductivity, and compatibility with diverse fabrication techniques [2]. Commonly used TCOs include titanium dioxide (TiO₂), indium oxide (In₂O₃), cesium carbonate (Cs₂CO₃), and zinc oxide (ZnO) [3]. ZnO, in particular, exhibits outstanding physicochemical characteristics such as a wide direct bandgap of 3.37 eV [4], high exciton binding energy (60 meV) [5], elevated electron mobility (205 cm². V-1.s-1) [6], and long electron lifetime [7]. In addition, its natural abundance, environmental friendliness, and chemical stability position ZnO as a highly attractive candidate for use in optoelectronic and photovoltaic applications. However, its properties are highly dependent on the synthesis technique used.

Thin films of Zinc oxide can be obtained by various techniques such as physical vapor deposition [8], magnetron sputtering [9], chemical vapor deposition [10], hydrothermal [11], doctor blade [12], electrodeposition [13], sonochemical [14], spray pyrolysis [15], chemical bath deposition [16] and sol-gel methods (dip-coating and spin-coating) [17, 18]. Among these, Spin coating is widely employed for the fabrication of ZnO thin films due to its simplicity and cost-effectiveness. The quality and performance of the resulting films strongly depend on processing parameters such as solvent type [19], spin speed [20], coating time [21], solution viscosity [22], and substrate properties [23]. Among these, spin speed plays a critical role, particularly in determining film thickness, morphology, crystallinity, surface and transparency [21]. However, despite its importance, the specific influence of spin speed on the structural and optical properties of ZnO thin films re-mains insufficiently addressed in existing studies, high-lighting the need for further investigation.

Several studies have addressed the influence of spin speed on ZnO films. For instance, Ajadi et al. [24] explored the effect of spin speeds ranging from 1000 to 6000 rpm

2077-6772/2025/17(5)05016(8)

05016-1

https://jnep.sumdu.edu.ua

^{*} Correspondence e-mail: mazbaneto@gmail.com

and observed a decrease in film thickness with increasing speed, with maximum transparency (88%) at 2000 rpm. Ilican et al. [25] analyzed ZnO films fabricated at 3000 – 5000 rpm, highlighting the impact of spin speed on optical band gap and crystallite size. Demircan et al. [21] focused on multilayer ZnO films and reported that both spin speed (2000 – 4000 rpm) and spin time significantly affected optical transmittance, film thickness, and electrical conductivity. They found that higher spin speeds produced thinner films with improved conductivity, while residual stress de-creased with increasing film thickness. However, most of these studies either focus on a limited number of spin parameters or lack a full cross-analysis of structural, morphological, and optical correlations.

Despite these contributions, the literature still presents notable gaps, particularly regarding the systematic evaluation of the spin speed effect on sol-gelderived multilayer ZnO films. Moreover, few studies provide a comprehensive correlation between spin speed and key functional properties, including orientation, surface crystallographic morphology, residual stress, transparency, and band gap energy, parameters that are essential for the effective integration of ZnO films into optoelectronic and photovoltaic devices.

This study provides a comprehensive analysis of the influence of spin speed on the structural, morphological, and optical properties of ZnO thin films deposited via solgel spin coating. The investigation aims to establish optimal processing conditions for achieving dense, uniform, and highly crystalline films suitable for electron transport applications in organic photovoltaic devices.

2.1 Materials and Reagents

In this study, microscope glass slides were used as substrates for the synthesis of ZnO thin films. All chemicals were of analytical reagent (AR) grade with a purity greater than 99 % and were used without further purification. Zinc acetate dihydrate [Zn(CH₃COO)₂ 2H₂O] served as the precursor, monoethanolamine (MEA) [HOCH₂CH₂NH₂] was used as the stabilizing agent, and 2-methoxyethanol [CH₃OCH₂CH₂OH] acted as the solvent. All chemicals were supplied by Thermo scientific. Ethanol (C₂H₆O), acetone [(CH₃)₂CO], and distilled water were used for cleaning the substrates prior to deposition.

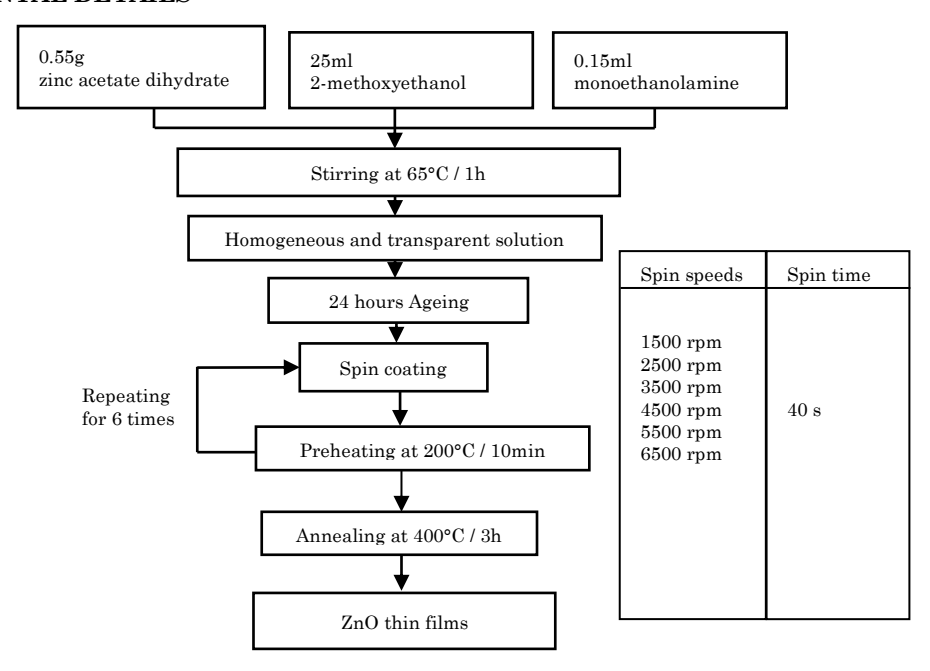
2.2 Substrate Cleaning

Substrate cleaning is a critical step to eliminate grease, dust, and other surface contaminants that can interfere with thin film adhesion and uniformity. In this study, microscope glass slides $(2.5~\text{cm}\times2~\text{cm})$ were cleaned sequentially in soapy water, distilled water, acetone, ethanol, and a final rinse in distilled water. Each step was performed for 10 minutes in an ultrasonic bath to ensure effective cleaning. Afterward, the substrates were dried in a laboratory oven.

2.3 Synthesis of ZnO Thin Films

ZnO thin films were deposited using spin coating method. The spin coating process typically involves three key stages: (i) application of the sol onto the substrate, (ii) rapid substrate rotation to ensure uniform spreading, and (iii) evaporation of the solvent during and after spinning.

2. EXPERIMENTAL DETAILS



 ${f Fig.~1}-{f Flow}$ chart of the synthesis process of ZnO thin films

Fig. 1 shows the flow chart for synthesizing ZnO thin films. A sol-gel solution with a concentration of 0.10 M was prepared by dissolving 0.55 g of zinc acetate dihydrate in 25 mL of 2-methoxyethanol. To ensure complete dissolution of the zinc salt, the solution was stirred using a magnetic stirrer for 10 minutes. Subsequently, 0.15 mL of MEA was gradually added with a micropipette in a 1:1 molar ratio with the zinc acetate. The mixture was then stirred at 65 °C for one hour until a homogeneous and transparent solution was obtained. Before deposition, the solution was aged for 24 hours at room temperature to allow complete dissolution of all solutes. Thin film synthesis was carried out on precleaned glass substrates using a spin coater (HOLMARC Model HO-TH-05) at spin speeds of 1500, 2500, 3500, 4500, 5500, and 6500 rpm for 40 seconds. After coating, the films were dried on a hot plate at 200 °C for 10 minutes to remove the solvent and organic residues. This coating and preheating were repeated six times for each spin speed. Finally, thermal treatment was performed to enhance film crystallinity. The samples were annealed at 400 °C for 3 hours to induce crystallization of ZnO.

2.4 Characterization of ZnO Thin Films

The crystalline structure of the synthesized ZnO thin films was analyzed using X-ray diffraction (XRD) with a Rigaku Ultima IV diffractometer equipped with Cu-Ka radiation ($\lambda = 1.5406\,\text{Å}$), operated at 30 kV and 15 mA. Scans were recorded in the 2θ range of 10° to 90°. Surface morphology was examined using a scanning electron microscope (SEM, ZEISS ULTRA 55 model), performed with a 1.5 kV operating voltage. The optical properties of the ZnO thin films were evaluated at room temperature using a UV-Visible spectrophotometer (UV-DT-MINI-2-GS model), with a spectral range of 300 – 900 nm.

3. RESULTS AND DISCUSSIONS

3.1 Structural Characterization

Fig. 2 presents the XRD patterns of ZnO thin films deposited at different spin speeds. The diffraction spectra display three peaks located at approximately $2\theta = 31.7^{\circ}$, 34.3° , and 36.8° , which correspond to the (100), (002), and (101) crystallographic planes, respectively. These peaks are characteristic of the hexagonal wurtzite structure of ZnO, in agreement with JCPDS card no. 36-1451 [26]. Moreover, no additional peaks associated with impurities are detected within the sensitivity limits of the XRD measurements, confirming that the films synthesized at different spin speeds consist of phase-pure ZnO.

The texture coefficient ($T_{C(hkb)}$) was determined for the three diffraction peaks using Eq. (1) in order to quantify the preferential orientation of ZnO crystallites [27]:

$$T_{C(hkl)} = \frac{\frac{I_{(hkl)}}{I_{0(hkl)}}}{\frac{1}{n} \sum_{I_{0(hkl)}}^{I_{(hkl)}}}$$
(1)

where $I_{(hkl)}$ are the XRD peak intensities obtained from

the films, $I_{0(hk)}$ are the peak intensities of the XRD reference (JCPDS card no. 36-1451) of the randomly oriented grains, and n the number of diffraction peaks considered.

As shown in Table 1, $T_{C(hkl)}$ values greater than 1 indicate a strong preferential orientation along the corresponding crystallographic plane [27]. Preferential growth along the (100) plane is observed at spin speeds of 1500, 2500, and 4500 rpm, suggesting that these conditions promote crystal alignment in this direction. In contrast, spin speeds of 3500, 5500, and 6500 rpm favor preferential growth along the (002) plane, indicating a change in the crystallite's orientation with increasing spin speed. This shift may result from crystallites reorganization driven by stronger centrifugal forces. These findings underscore the critical role of spin speed in tailoring the structural texture of ZnO thin films.

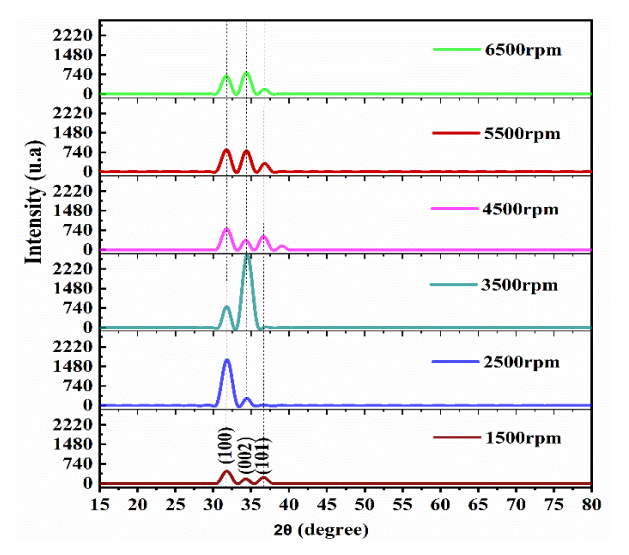


Fig. 2 – XRD patterns of ZnO thin films elaborated with different spin speeds

The plane d-spacing (d_{hkl}) and the lattice parameters (a and c) of the synthesized ZnO thin films were calculated according to Bragg's law, as expressed in Eq. (2) and Eq. (3), respectively [28]:

$$d = \frac{\lambda}{2\sin\theta} \tag{2}$$

$$a = \sqrt{\frac{1}{3}} \frac{\lambda}{\sin \theta}$$
 and $c = \frac{\lambda}{\sin \theta}$ (3)

Where λ is CuK α wavelength (1.54059Å) and θ is the diffraction peak angle.

The lattice parameters a and c, listed in Table 1, exhibit slight fluctuations but remain close to the standard values reported in JCPDS card No. 36-1451 for ZnO [26]. These minor variations can be attributed to shifts in the diffraction peak positions 2θ (Table 1). Nevertheless, the c/a ratio for all samples remains around 1.60, which corresponds to the ideal value for bulk wurtzite ZnO [29]. This stability in the c/a ratio suggests that the films maintain the wurtzite crystal structure without notable distortion or phase

transformation during the deposition process. It also implies a dense and orderly atomic arrangement, which enhances both the mechanical integrity and electronic performance of the films [30]. Moreover, the near-ideal ratio points to a low defect density, indicating high crystallinity and minimal lattice irregularities [31]. Additionally, as shown in Table 1, the interplanar spacing (d), calculated using Bragg's law, remains nearly constant across all diffraction planes and closely aligns with the standard JCPDS values. This consistency further confirms the structural stability of the ZnO thin films throughout the deposition process.

The crystallite sizes (D) of the films along the three peaks (100), (002) and (101) were calculated using Debye Scherer formula presented by Eq. (4) [32]:

$$D = \frac{k\lambda}{\beta\cos\theta} \tag{4}$$

where k = 0.9, θ is the XRD diffraction peak angle, $\lambda = 1.54059$ Å is the X-ray wavelength and β is the full width at half peak (FWHM) in radians.

The dislocation density (δ) which induces the defects in crystal is estimated by Eq. (5) [32]:

$$\delta = \frac{1}{D^2} \tag{5}$$

The crystallite size (D) at 2500 rpm, particularly for

31.770

card 1451 34.422

the (100) plane, with a maximum size of $D=43.803\,\mathrm{nm}$, implying larger and better-organized grains. As the speed increases beyond 3500 rpm, crystallite size gradually decreases, likely due to increased centrifugal forces, faster solvent evaporation, and higher internal stress, which limit the time available for grain growth [19]. The dislocation density (δ), which is inversely related to crystallite size, is lowest at 2500 rpm for the (100) plane, reflecting a low density of crystalline defects and thus higher structural quality. At 3500 rpm, the dislocation density is minimized along the (002) plane, consistent with improved crystallinity. However, at 6500 rpm, δ increases sharply, indicating more structural defects due to excessive rotational energy.

The internal strain components along the a- and c-axes, denoted as ε_a and ε_c , were calculated using Eqs. (6) and (7), respectively [33].

$$\varepsilon_a = \frac{a - a_0}{a_0} \times 100\% \tag{6}$$

$$\varepsilon_c = \frac{c - c_0}{c_0} \times 100\% \tag{7}$$

where $a_0 = 3.249$ Å and $c_0 = 5.206$ Å constants of the standard unconstrained ZnO lattice given by JCPDS card 36-1451 [26].

| Spin speeds | 2θ(°) | | | $T_{C(hkl)}$ | | | Lattice parameters | | c/a | d_{nkl} (Å) | | |
|----------------|--------|--------|--------|--------------|-------|-------|--------------------|-------|-------|---------------|-------|-------|
| | (100) | (002) | (101) | (100) | (002) | (101) | a (Å) | c (Å) | ratio | (100) | (002) | (101) |
| 1500 rpm | 31.813 | 34.315 | 36.674 | 0.918 | 1.059 | 1.023 | 3.245 | 5.222 | 1.609 | 2.812 | 2.611 | 2.448 |
| 2500 rpm | 31.726 | 34.492 | 36.836 | 2.395 | 0.595 | 0.009 | 3.254 | 5.196 | 1.596 | 2.818 | 2.598 | 2.438 |
| 3500 rpm | 31.751 | 34.280 | 36.748 | 0.575 | 2.394 | 0.030 | 3.252 | 5.227 | 1.598 | 2.815 | 2.614 | 2.444 |
| 4500 rpm | 31.753 | 34.300 | 36.648 | 1.562 | 0.838 | 0.600 | 3.251 | 5.224 | 1.606 | 2.816 | 2.612 | 2.450 |
| 5500 rpm | 31.705 | 34.387 | 36.824 | 1.268 | 1.456 | 0.276 | 3.256 | 5.212 | 1.601 | 2.819 | 2.605 | 2.438 |
| 6500 rpm | 31.698 | 34.382 | 36.816 | 1.144 | 1.639 | 0.216 | 3.257 | 5.213 | 1.600 | 2.820 | 2.606 | 2.439 |
| JCPDS | | | | | | | | | | | | |

3.250

5.207

1.602

2.814

2.603

2.476

 $\textbf{Table 1} - \text{Diffraction angles, texture coefficient, lattice parameters and plane d-spacing of ZnO thin films deposited at different spin speeds and the plane of the parameters and plane of the parameters are parameters and plane of the parameters and plane of the parameters are parameters are parameters and plane of the parameters are parameters are parameters and plane of the parameters are parameters and plane of the parameters are para$

Table 2 - Other structural characteristics of ZnO thin films deposited at different spin speeds

36.253

| Spin speeds | β (°) | | | D (nm) | | | δ (×10 ¹⁵ lines/m²) | | | Internal strains along a and c axis | | V (Å3) | L (Å) |
|----------------|-------|-------|-------|--------|--------|--------|---------------------------------------|-------|--------|---|------------------|--------|-------|
| speeds | (100) | (002) | (101) | (100) | (002) | (101) | (100) | (002) | (101) | ε_a (%) | ϵ_c (%) | | |
| 1500 rpm | 0.504 | 0.531 | 0.843 | 16.383 | 15.661 | 9.927 | 3.725 | 4.076 | 10.147 | 0.136 | -0.303 | 47.637 | 1.406 |
| 2500 rpm | 0.188 | 0.370 | 0.414 | 43.803 | 22.427 | 20.217 | 0.521 | 1.988 | 2.446 | -0.131 | 0.196 | 47.653 | 1.407 |
| 3500 rpm | 0.539 | 0.612 | 0.501 | 15.313 | 13.570 | 16.696 | 4.264 | 5.430 | 3.587 | -0.054 | 0.165 | 47.595 | 1.406 |
| 4500 rpm | 0.512 | 0.568 | 0.574 | 16.109 | 14.631 | 14.577 | 3.853 | 4.671 | 4.705 | -0.048 | -0.345 | 47.832 | 1.407 |
| 5500 rpm | 0.498 | 0.533 | 0.589 | 16.554 | 15.597 | 14.194 | 3.649 | 4.110 | 4.963 | -0.196 | -0.099 | 47.855 | 1.408 |
| 6500 rpm | 0.538 | 0.551 | 0.689 | 15.324 | 15.079 | 12.147 | 4.258 | 4.398 | 6.776 | -0.217 | -0.114 | 47.883 | 1.408 |

Tables 2 shows variations in the internal strain values (ε_a and ε_c) of ZnO thin films deposited at different spin speeds. These changes are primarily attributed to lattice mismatch and stacking defects between the ZnO crystal structure and the underlying glass substrate [33, 34]. Such imperfections induce distortions in the lattice, which manifest as internal strain within the thin films. A positive internal strain indicates tensile stress, meaning the lattice parameters are expanded relative to their equilibrium values. This may result from thermal effects, oxygen vacancies, or film-substrate interaction during deposition [16]. Conversely, a negative strain corresponds to compressive stress, reflecting a contraction of the lattice parameters due to structural constraint or limited relaxation during film formation [35].

The structural parameters, including the volume (V) of the hexagonal wurtzite unit cell and the Zn-O bond length (L), were derived from Eqs. (8) and (9), respectively [36].

$$V = \left(\frac{\sqrt{3}}{2}\right)a^2c \tag{8}$$

$$L = \sqrt{\frac{a^2}{3} + \left(\frac{1}{2} - u\right)^2 c^2} \tag{9}$$

where the parameter (u), representing the internal

atomic displacement along the c-axis in the hexagonal wurtzite structure, was evaluated using Eq. [36]:

$$u = \frac{a^2}{3c^2} + 0.25\tag{10}$$

Table 2 presents slight variations in the Zn-O bond length (L) and the unit cell volume (V) of the hexagonal wurtzite structure. These changes are directly related to shifts in 2θ , as both L and V depend on the lattice parameters a and c [33]. Since diffraction peaks are highly sensitive to lattice dimension changes, any fluctuation in a and c will consequently influence the bond length and unit cell volume of the ZnO thin films [33].

3.2 Morphological Properties

To investigate the surface morphology of the ZnO thin films, scanning electron microscopy (SEM) was carried out, and the results are shown in Fig. 3. At a spin speed of 1500 rpm (Fig. 3a), the film dis-played a rough, heterogeneous surface, characterized by large aggregates and noticeable irregularities. This morphology reflects the insufficient centrifugal force at low spin speed, which limits the uniform distribution of the sol-gel solution across the substrate.

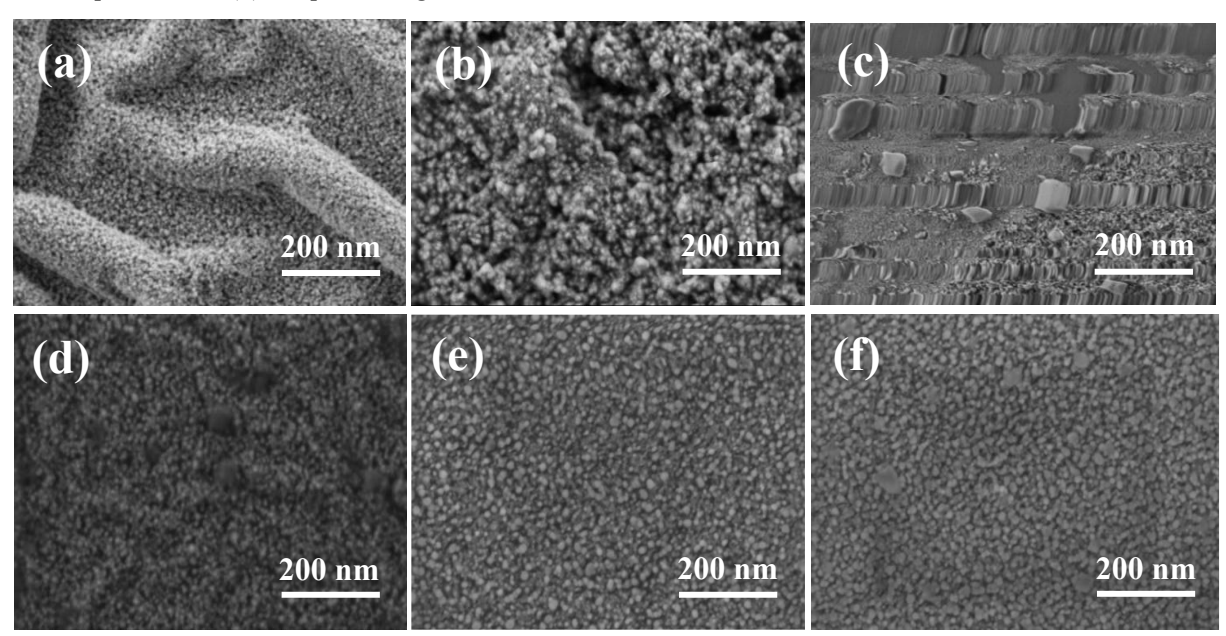


Fig. 3 – SEM images of ZnO thin films developed with different spin speeds: (a) 1500 rpm, (b) 2500 rpm, (c) 3500 rpm, (d) 4500 rpm, (e) 5500 rpm and (f) 6500 rpm

As the spin speed increased to 2500 rpm (Fig. 3b), a reduction in grain size was observed, along with partial improvement in surface uniformity. However, the morphology still exhibited some disorder. At 3500 rpm (Fig. 3c), the surface began to exhibit directional features, suggesting that the in-creased centrifugal force played a more significant role in aligning and orienting the deposited particles. This marks a transition toward more organized film formation.

At 4500 rpm (Fig. 3d), the morphology became notably denser and more homogeneous, with fine grains uniformly covering the surface, indicating a substantial improvement in film quality. This trend continued at 5500 rpm (Fig. 3e), where the films appeared smooth, compact, and nearly free of visible defects. This condition seems optimal, achieving a balance between compactness, uniformity, and good substrate adhesion.

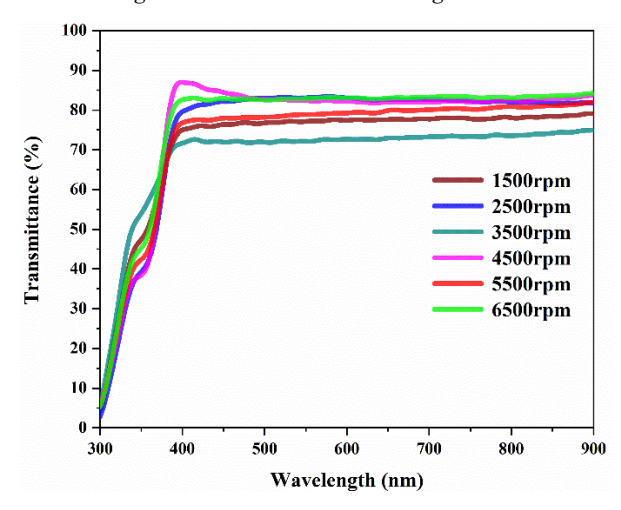
However, at 6500 rpm (Fig. 3f), although the

microstructure remained fine, a slight decrease in surface density and cohesion was noted. This may be attributed to excessive centrifugal force, which could lead to partial film detachment or microstructural instability, potentially affecting long-term adhesion and mechanical integrity [21].

Overall, the findings demonstrate that increasing the spin speed enhances the spreading of the sol-gel solution and accelerates solvent evaporation [19]. These conditions facilitate the formation of smaller, more uniform grains, an essential characteristic for enhancing charge transport and overall performance in photovoltaic applications (e.g., reduced surface defects and improved film compactness) [37]. Moreover, these SEM observations are consistent with the XRD results, confirming the improved structural quality of ZnO thin films at higher spin speeds.

3.3 Optical Properties

Fig. 4 shows the UV-visible transmittance spectra of ZnO thin films in the 300-900 nm wave-length range for various spin speeds. All films display high transmittance in the visible region, consistently above 70 %, with a peak value of approximately 85 % at 6500 rpm. An increase in spin speed leads to a gradual enhancement in transmittance and a sharper absorption edge that shifts toward shorter wave-lengths (blue shift). This behavior suggests a widening of the optical bandgap (E_g), typically associated with improved crystallinity and reduced structural defects such as oxygen vacancies [38]. The improved transparency at higher spin speeds is likely due to enhanced film uniformity and lower defect density, corroborating the XRD and SEM findings.



 ${\bf Fig.~4}-{\bf Transmittance}$ spectra of ZnO thin films deposited at different spin speeds

To further investigate the optical bandgap, Fig. 5 presents the first derivative of the transmittance spectra with respect to wavelength, plotted against photon energy. The peak positions of the derivative curves, corresponding to the most prominent optical transitions, were used to estimate E_g values, which varied between

3.28 and 3.32 eV, as listed in Table 3. These slight variations are attributed to differences in crystallite size and structural disorder [39]. Smaller grains may induce quantum confinement effects, resulting in a higher bandgap [40], while structural imperfections, such as oxygen vacancies and zinc interstitials, can introduce localized energy states that modify optical transitions [41]. Additionally, internal strain and the nanostructured morphology of the films may contribute to the observed shifts through optical confinement effects [41, 42].

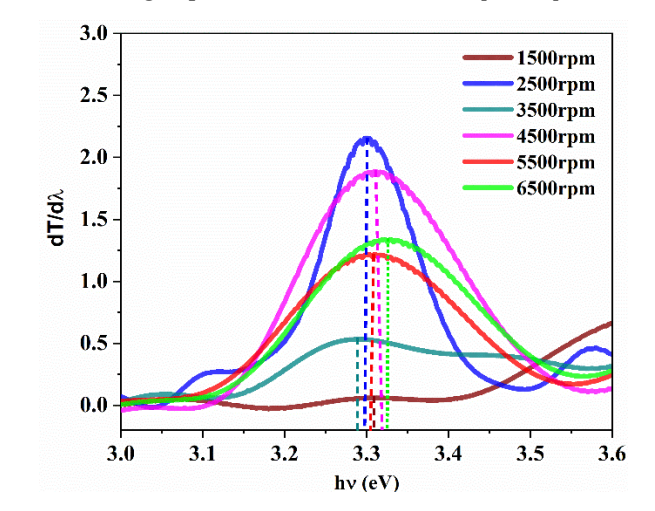


Fig.5 – $dT/d\lambda$ versus photon energy curves for ZnO thin films deposited at different spin speeds.

Table 3 – Bandgap values of ZnO thin films deposited at different spin speeds

| Spin speeds | Gap energy (eV) | | | | | |
|-------------|-----------------|--|--|--|--|--|
| 1500 rpm | 3.30 | | | | | |
| 2500 rpm | 3.29 | | | | | |
| 3500 rpm | 3.28 | | | | | |
| 4500 rpm | 3.31 | | | | | |
| 5500 rpm | 3.30 | | | | | |
| 6500 rpm | 3.32 | | | | | |

4. CONCLUSION

ZnO thin films were successfully synthesized on glass substrates using the sol-gel spin-coating method at varying spin speeds. XRD analysis confirmed the formation of a polycrystalline hexagonal wurtzite structure, with a notable shift in preferential orientation from the (100) plane at lower spin speeds (1500, 2500, 4500 rpm) to the (002) plane at higher speeds (3500, 5500, 6500 rpm). This change reflects the influence of centrifugal forces and solvent evaporation kinetics on the crystal growth mechanism. SEM analysis revealed that increasing the spin speed leads to improved surface morphology, transitioning from rough, inhomogeneous films at low speeds to smooth and compact structures at higher speeds (≥ 4500 rpm), owing to more effective solution spreading and faster solvent evaporation. UVspectroscopy demonstrated high

transparency (72-85%) in the visible region, with the highest transmittance observed at 6500 rpm. The optical bandgap varied slightly between 3.28 and 3.32 eV, reflecting subtle differences in film crystallinity and defect concentration. Overall, spin speed was shown to be a critical parameter in tuning the structural, morphological, and optical properties of ZnO thin films. The findings highlight optimal processing windows for

producing high-quality ZnO films suitable for applications in optoelectronic and photovoltaic applications.

AKNOWLEDGEMENTS

We would like to express our sincere gratitude to CERME (Togo) for the financial support and Universitat Politècnica de València (Spain) for formal analysis.

REFERENCES

- 1. F.U. Hamelmann, J. Phys.: Conf. Ser. 559, 012016 (2014).
- H. Hosono, K. Ueda, Springer International Publishing, Cham, 1391 (2017).
- T. Li, Z. Chen, Y. Wang, et al., ACS Appl. Mater. Interfaces 12, 3301 (2020).
- V. Parihar, M. Raja, R. Paulose, Rev. Adv. Mater. Sci. 53, 119 (2018).
- 5. N.K. Hassan, M.R. Hashim, Y. Al-Douri, *Optik* 125, 2560 (2014).
- D.C. Look, D.C. Reynolds, J.R. Sizelove, et al., Solid State Commun. 105, 399 (1998).
- S. Aksoy, O. Polat, K. Gorgun, et al., *Physica E* 121, 114127 (2020).
- A. George, P. Kumari, N. Soin, et al., Mater. Chem. Phys. 123, 634 (2010)
- O. Lupan, V.M. Guérin, L. Ghimpu, et al., Chem. Phys. Lett. 550, 125 (2012).
- N. Schaper, D. Alameri, Y. Kim, et al., *Nanomaterials* 11, 1836 (2021).
- K. Elen, H. Van Den Rul, A. Hardy, et al., Nanotechnology 20, 055608 (2009).
- K. Magiswaran, M.N. Norizan, N. Mahmed, et al., *Coatings* 13, 20 (2022).
- S. Xu, D. Fang, F. Xiong, et al., *J. Solid State Electrochem.* 28, 589 (2023).
- A. Khorsand Zak, abd. W.H. Majid, H.Z. Wang, et al., *Ultrason. Sonochem.* 20, 395 (2013).
- O. Ako, M. Baneto, M. Senthilkumar, et al., *Int. J. Renew. Energy Dev.* 14 No 3, 495 (2025).
- A.D. Gboglo, M. Baneto, K.S. Gadedjisso-Tossou, et al., Surfaces 8 No 3, 46 (2025).
- 17. Y. Natsume, H. Sakata, *Thin Solid Films* 372, 30 (2000).
- K. Wojtasik, M. Zięba, C. Tyszkiewicz, et al., *Materials* 16, 1898 (2023).
- K.D.A. Kumar, S. Valanarasu, A. Kathalingam, et al., *Appl. Phys. A* 123, 801 (2017).
- Motlan, N. Siregar, J.H. Panggabean, J Phys. Conf. Ser. 1819, 012050 (2021).
- G. Demircan, E.F. Gurses, A. Acikgoz, et al., *Mol. Cryst. Liq. Cryst.* 709, 61 (2020).

- J.-K. Hong, H.-R. Kim, H.-H. Park, *Thin Solid Films* 332, 449 (1998).
- W. Yang, J. Liu, M. Liu, et al., Superlattice. Microstr. 136, 106291 (2019).
- 24. D.A. Ajadi, S.M. Agboola, O. Adedokun, MSCE 04, 1 (2016).
- S. Ilican, Y. Caglar, M.Caglar, J. Optoelectron. Adv. Mater. 10 No 10, 2578 (2008).
- H.F. McMurdie, M.C.Morris, E.H.Evans, et al., Powder Diffr. 1, 64 (1986).
- R. Romero, D. Leinen, E.A. Dalchiele, et al., *Thin Solid Films* 515, 1942 (2006).
- M. Kashif, U. Hashim, M.E. Ali, et al., J. Nanomater. 2012, 452407 (2012).
- H. Morkoç, Ü. Özgür, Zinc Oxide: Fundamentals, Materials and Device Technology (John Wiley & Sons: 2008).
- B.M. Nizar, M. Lajnef, J. Chaste, et al., RSC Adv. 13, 15077 (2023).
- A.U.H.S. Rana, S.F. Shaikh, A.M. Al-Enizi, et al., *Nanomaterials* 10, 142 (2020).
- S. Mustapha, M.M. Ndamitso, A.S. Abdulkareem, et al., Adv. Nat. Sci. Nanosci. Nanotechnol. 10, 045013 (2019).
- 33. A.F. Abdulrahman, S.M. Ahmed, N.M. Ahmed, M.A. Almessiere, *Crystals* 10, 386 (2020).
- M. Narasimha Murthy, C.J. Sreelatha, G. Ravinder, S. Anusha, *Mater. Today: Proc.* 54, 602 (2022).
- N. Rosli, M.M. Halim, M.R. Hashim, Appl. Phys. A 127, 712 (2021).
- A.F. Abdulrahman, S.M. Ahmed, S.M. Hamad, et al., *Chin. J. Phys.* 71, 175 (2021).
- 37. H. Lee, X. Zhang, J. Hwang, J. Park, *Materials* **9**, 851 (2016).
- 38. J. Wang, Z. Wang, B. Huang, et al., ACS Appl. Mater. Interface.
- E.M. Wong, P.C. Searson, Appl. Phys. Lett. 74, 2939 (1999).
- F.N.C. Anyaegbunam, C. Augustine, Digest Journal of Nanomaterials and Biostructures 13, 847 (2018).
- 41. R. Marotti, Sol. Energy Materi. Sol. C. 82, 85 (2004).
- K.L. Foo, U. Hashim, K. Muhammad, C.H. Voon, Nanoscale Res. Lett. 9, (2014).

Контрольоване осадження тонких плівок ZnO методом спінінгового покриття: вплив швидкості спінінгу на мікроструктуру та прозорість плівки

M. Baneto^{1,2}, D. Djagbai^{1,2}, E. Mouzou^{1,2,3}, A.D. Gboglo^{1,2}, O. Ako^{1,2}, M.F. Kouide^{1,2}, D. Kassegne^{1,2}

Centre d'Excellence Régional pour la Maîtrise de l'Electricité (CERME), University of Lomé, 01BP 1515 Lomé, Togo
 Laboratory on Solar Energy, Department of Physics, Faculty of Sciences, University of Lomé, 01BP 1515 Lomé, Togo
 Physics of Semiconductor Materials and Components Laboratory, Department of Physics, Faculty of Sciences,
 University of Lomé, 01BP 1515 Lomé, Togo

Тонкі плівки оксиду цинку (ZnO) були синтезовані на скляних підкладках методом золь-гель спінпокриття для дослідження впливу швидкості обертання підкладки на її структурні, морфологічні та
оптичні властивості. Дигідрат ацетату цинку, 2-метоксиетанол та моноетаноламін використовувалися як
прекурсор, розчинник та стабілізатор відповідно. Процес нанесення покриття проводився при швидкостях
обертання від 1500 до 6500 об/хв протягом 40 секунд. Потім плівки попередньо нагрівали при 200 °C
протягом 10 хвилин та відпалювали при 400 °C протягом 3 годин. Рентгенівський дифракційний аналіз
підтвердив, що всі плівки мали полікристалічну гексагональну структуру вюрциту. Скануюча електронна
мікроскопія показала, що морфологія плівок значно залежить від швидкості обертання: низькошвидкісні
покриття призводили до шорстких, неоднорідних поверхонь, тоді як вищі швидкості (≥ 4500 об/хв)
утворювали гладкі, однорідні плівки. УФ-видима спектроскопія показала, що всі зразки зберігали високу
прозорість (понад 70%) у видимій області, з найвищим коефіцієнтом пропускання (85%), що спостерігався
при 6500 об/хв. Оптична заборонена зона варіювалася від 3,28 до 3,32 еВ залежно від швидкості
обертання. Ці результати підкреслюють придатність тонких плівок ZnO, нанесених методом обертання,
для застосування у прозорих електродах фотоелектричних приладах.

Ключові слова: Тонкі плівки, Оксид цинку, Мікроструктура, Центрифугування, Швидкість центрифугування, Фотоелектричні застосування.